Article

Outstanding Performance of Transition-Metal-Decorated Single-Layer Graphene-like BC$_6$N Nanosheets for Disease Biomarker Detection in Human Breath

Aref Aasi, Sadegh Mehdi Aghaei,* and Balaji Panchapakesan*
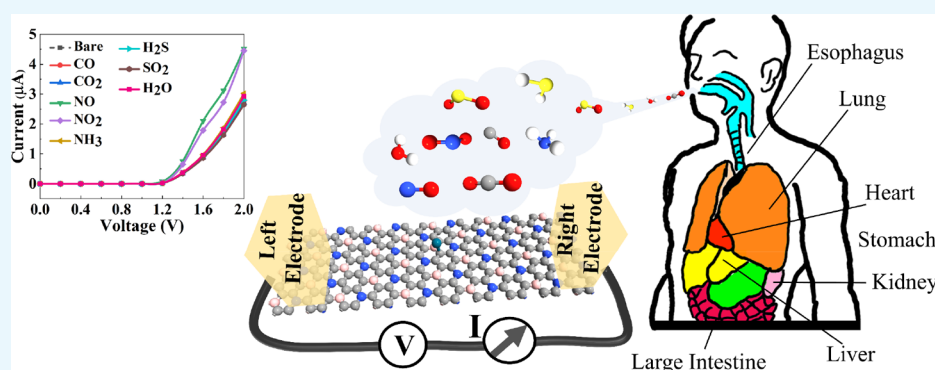
Read Online

ACCESS | Metrics & More | Article Recommendations | SI Supporting Information

ABSTRACT: In the present work, we report highly sensitive and selective nanosensors constructed with metal-decorated graphene-like BC$_6$N employing nonequilibrium Green's function (NEGF) formalism combined by density functional theory (DFT) toward multiple inorganic and sulfur-containing gas molecules (NO, NO$_2$, NH$_3$, CO, CO$_2$, H$_2$S, and SO$_2$) as disease biomarkers from human breath. Monolayer sheets of pristine BC$_6$N and Pd-decorated BC$_6$N were evaluated for their gas adsorption properties, electronic property changes, sensitivity, and selectivity toward disease biomarkers. The pristine BC$_6$N nanosheets exhibited sharp drops in the bandgap when interacted with gases such as NO$_2$ while barely affected by other gases. However, the nanosecond recovery time and low adsorption energies limit the gas sensing applications of the pristine BC$_6$N sheet. On the other hand, the Pd-decorated BC$_6$N-based sensor underwent a semiconductor to metal transition upon the adsorption of NO$_x$ gas molecules. The conductance change of the sensor's material in terms of I−V characteristics revealed that the Pd-decorated BC$_6$N sensor is highly sensitive (98.6−134%) and selective (12.3−74.4 times) toward NO$_x$ gas molecules with a recovery time of 270 s under UV radiation at 498 K while weakly interacting with interfering gases in exhaled breath such as CO$_2$ and H$_2$O. The gas adsorption behavior suggests that metal-decorated BC$_6$N sensors are excellent candidates for analyzing pulmonary disease and cardiovascular biomarkers, among other ailments of the stomach, kidney, and intestine.

INTRODUCTION

Graphene, a two-dimensional (2D) honeycomb lattice of monolayer carbon atoms,[1] has triggered intensive research interest due to its outstanding electrical transport, optical, and thermal properties.[2] Considered as a basic building block to all other dimensionalities, multiple graphene sheets can be stacked together to create three-dimensional (3D) graphite. A graphene sheet can be rolled up to form one-dimensional (1D) carbon nanotubes or can be wrapped up to produce zero-dimensional (0D) fullerenes.[3] Nevertheless, the applications of pristine graphene in post-silicon nanoelectronics and sensors are limited due to its zero-energy bandgap. To overcome this limitation, different approaches for modifying the electronic structure of graphene have been proposed such as doping,[4,5] decoration by transition-metal atoms,[6−8] etc. On the other hand, new 2D semiconductor materials such as MoS$_2$,[9] WS$_2$,[10]

and phosphorene,[11] among others, are being increasingly researched today.

The possibility of producing n-type and p-type semiconducting graphene by substituting C atoms with nearest-neighbor N and B atoms seems like a tantalizing approach toward the realization of nanodevices.[12,13] Boron and nitrogen can form strong covalent bonds with carbon owing to their atomic size and being the nearest neighbor to carbon in the periodic table. Carbon nitrides (C$_3$N) and boron carbides

(BC_3) show semiconducting behavior and retain the mechanical properties of graphene due to the covalent network of C and N or B atoms.[14] More excitingly, the semiconducting hexagonal layered structures with different stoichiometries can be formed by mixing B, C, and N elements.[15] Recently, BC_6N (borocarbonitride) as a transition structure between the C_3N and BC_3 lattices was directly synthesized using a two-step borylation reaction.[16] Despite having a geometric structure almost identical to graphene, BC_6N exhibits semiconducting characteristics with a direct bandgap of 1.28 eV.[17,18] It is expected that the electronic properties of BC_6N structures can be engineered thanks to the donor behavior of N atoms and acceptor behavior of B atoms.[19] Furthermore, due to the high concentration of C atoms, BC_6N retains the physical properties of graphene and offers high carrier mobility, mechanical properties, and high thermal conductivity, making it a promising material for nanoelectronics and sensor applications.[20] Despite its excellent physical properties, there is a very limited understanding of how BC_6N interact with gases in pristine and metal-decorated configurations for detecting disease biomarkers from human breath.

There are many components in exhaled breath, which can be classified as volatile organic compounds (VOCs), inorganic compounds, volatile sulfuric compounds (VSCs), and other compounds that can be used to identify disease states.[21] Recent reports have shown the possibility of testing human breath for the detection of serious illnesses like different types of cancers and lung, kidney, and Alzheimer's diseases, to name a few.[22] Carbon-based nanomaterials have been extensively investigated toward breath analysis.[23−26] Here, potential applications of graphene-like single-layer pristine BC_6N sheets and their metal-decorated counterparts could be useful as arrays of room temperature gas sensors for smartphone breath analysis. The advantages of graphene-like semiconducting materials and their metal-decorated counterparts include nanodevice configuration that can have exceptional sensitivity and selectivity to few molecules, fast response in milliseconds to seconds, quick recovery, an ability to program the devices, and low cost using batch manufacturing.[27] Past work has shown that BC_3 nanotubes have the capability of detecting various hazardous gases such as CO.[28] C_3N was also introduced as a platform for the sensing of NO_2 with good sensitivity and selectivity.[29] Moreover, it was reported that doping impurities such as Al and Si in BC_3 structures could improve the adsorption of molecules like formaldehyde (H_2CO).[30]

Our work introduces a simple metal (palladium, Pd)-decorated BC_6N system as molecular sensors for room temperature breath analysis. Taking advantage of local charges induced by B and N atoms and the catalytic effect of the metal atoms, pristine BC_6N and metal (Pd)-decorated BC_6N were investigated in different inorganic and sulfur-containing gas molecules in exhaled breath such as NO, NO_2, NH_3, CO, CO_2, H_2S, and SO_2 comprehensively using first-principles methods based on nonequilibrium Green's function (NEGF) formalism in combination with density functional theory (DFT). We found that pristine BC_6N selectively detects NO_x gas molecules owing to the measurable alteration in its electronic transport properties after gas exposure. It was discovered that the decoration of the BC_6N sheet by Pd atoms could simultaneously improve the selectivity and sensitivity toward the NO_x gas molecules. A 12 to 70 times enhancement in selectivity toward NO_x over CO_2 and humidity was achieved,

conclusively indicating that metal-decorated BC_6N is a promising material for detecting breath biomarkers.

RESULTS AND DISCUSSION

We first studied the structure of pristine monolayer graphene-like BC_6N. The energy-minimized configuration of BC_6N and its hexagonal unit cell with a lattice constant of 4.99 Å is shown in Figure 1a, where a C hexagon (6 atoms) is linked to an N
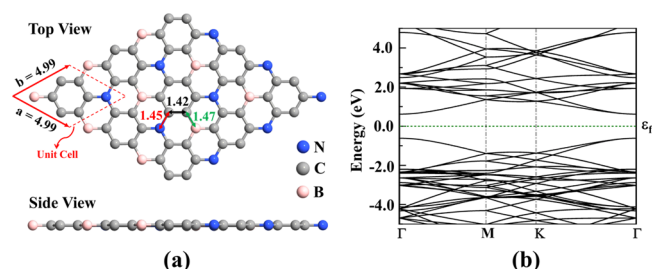

Figure 1. (a) Top and side view of the pristine hexagonal BC_6N sheet and its unit cell. (b) Band structure plot of pristine BC_6N.

atom and a B atom. The optimized structure of graphene-like BC_6N has planar geometry (sp^2 hybridization). The C−C bond length is 1.42 Å, the C−B bond length is 1.47 Å, and the C−N bond length is 1.45 Å. As can be seen in Figure 1b, BC_6N is a direct bandgap semiconductor (E_g = 1.228 eV), in excellent agreement with the literature.[18,31,32] We note that the AIMD and phonon spectrum simulations performed in ref 33 at 300 K showed thermal and dynamic stabilities of the BC_6N sheet.

A 3 × 3 supercell was used to model and analyze the interaction between the 2D BC_6N sheet and the gas molecules. Various adsorption sites (above C hexagons, B−N−C hexagons, a C−C bond, a C−B bond, a C−N bond, and C, B, and N atoms) and different molecular orientations (perpendicular or parallel to the BC_6N surface) were studied. In addition, for diatomic molecules such as CO and NO in the perpendicular configuration, the O atom can point to or away from the surface of BC_6N. For triatomic molecules (CO_2, NO_2, SO_2, H_2S, and H_2O) and a tetratomic molecule (NH_3) in perpendicular configuration, the O atoms (in CO_2, NO_2, and SO_2) and the H atoms (in NH_3, H_2S, and H_2O) could point up or down. Therefore, a number of configurations were considered as input geometries and fully optimized. The interaction strength between sensing materials and analytes was evaluated by calculating adsorption energies. The negative adsorption energy is indicative of exothermic adsorption, and the more negative value of adsorption energy refers to the stronger interaction between the adsorbate and the adsorbent. The most stable adsorption geometries were selected for further studies (see Figure 2).

Upon exposure to CO and NO, they both adopt a vertical configuration to the C hexagon of BC_6N. The interaction distance (shortest atom−atom distance between gas molecules and the BC_6N sheet) for the CO−BC_6N structure was estimated to be 2.84 Å, which is the distance between the O atom of CO and BC_6N (O−C), and the shortest distance between the N atom of NO and BC_6N (N−C) was calculated to be 2.49 Å. A CO_2 molecule was adsorbed in a parallel orientation above the B−C bond, where the shortest distance between the O atom of CO_2 and BC_6N (O−C) was found to be 2.95 Å. The NO_2 and H_2S gas molecules preferred to be
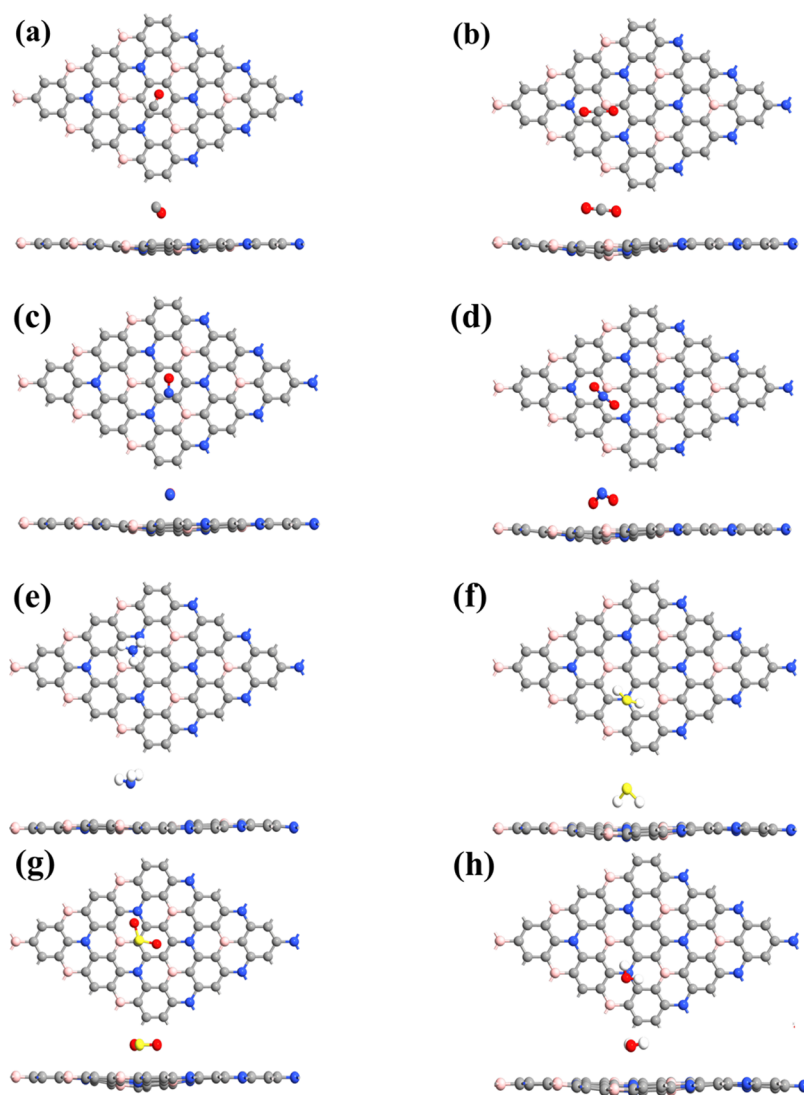
Figure 2. Most stable adsorption geometries of the pristine BC_6N sheet exposed to (a) CO, (b) CO_2, (c) NO, (d) NO_2, (e) NH_3, (f) H_2S, (g) SO_2, and (h) H_2O. Pink, gray, blue, red, yellow, and white balls represent B, C, N, O, S, and H atoms, respectively.

adsorbed in vertical orientations. NO_2 was placed above the B−C bond with the O atom pointing down, and the shortest distance between the O atom of NO_2 and BC_6N (O−C) was 2.56 Å. In addition, H_2S was positioned above the N atom of BC_6N with the H atom pointing down, and the shortest distance between the H atom of H_2S and BC_6N (H−C) was 2.40 Å. Upon interaction of NH_3 with the BC_6N sheet, the N atom of the molecule pointed down toward the B−C−N hexagon, where the shortest distance between the N atom of NH_3 and BC_6N (N−N) was found to be 3.27 Å. Finally, SO_2 and H_2O were absorbed in a parallel configuration with respect to BC_6N. SO_2 was located above the C atom with the shortest distance (S−C) of 2.79 Å. Also, H_2O was placed above the N atom with the shortest distance between the O atom of H_2O and BC_6N (O−N) of 2.88 Å.

The atomic radii of B, C, N, O, S, and H atoms are 0.87, 0.67, 0.56, 0.48, 0.88, and 0.53 Å, respectively.[34] The minimum distance between the BC_6N sheet and CO (C−O), CO_2 (C−O), NO (C−N), NO_2 (C−O), NH_3 (N−N), H_2S (C−H), SO_2 (C−S), and H_2O (O−N) were found to be 2.84, 2.95, 2.49, 2.56, 3.27, 2.40, 2.79, and 2.88 Å, respectively. Moreover, the sums of corresponding atomic radii are 1.15, 1.15, 1.23,

1.15, 1.12, 1.2, 1.55, and 1.04 Å, respectively. Therefore, the minimum distances between the BC_6N sheet and the molecules are greater than the sums of corresponding atomic radii, suggesting that gas molecules and BC_6N sheet interactions are governed by physisorption.

The values of adsorption energies for gas molecules upon interaction with pristine BC_6N were found to be −0.22, −0.225, −0.311, −0.265, −0.264, −0.26, −0.483, and −0.258 eV, for CO, CO_2, NO, NO_2, NH_3, H_2S, SO_2, and H_2O, respectively. These small adsorption energies confirm that all gases are physisorbed; however, they are adequate to endure thermal disturbance at room temperature ($K_BT \cong 25$ meV). Due to lack of chemical interactions, CO, CO_2, NO, NH_3, and H_2O molecules correspondingly donate a small charge of 0.012, 0.015, 0.071, 0.026, and 0.015 e to the BC_6N sheet. Though, NO_2, H_2S, and SO_2 molecules withdraw a small charge of 0.071, 0.044, and 0.073 e from the BC_6N sheet, respectively.

As can be seen from Figure 2, the BC_6N sheet experienced a slight deformation after the adsorption of analytes. The deformation energies can be calculated using[35,36]

Table 1. The Gas Molecule Adsorption Energy (E_{ad}) on the Adsorbent in eV, the Interaction Distance (D) between the Gas Molecules and the Adsorbent Surface in Å, Charge Transfer (Q) between Gas Molecules and the Adsorbent in e, the Energy Bandgap (E_g) in eV, Recovery Time (τ) in Different Conditions in s, Deformation Energy (E_{def}) in eV, and Magnetic Moment (m) in μ_B

system	E_{ad} (eV)	D (Å)	Q (e)	E_g (eV)	τ (s) @ T = 298 K (visible light)	τ (s) @ T = 498 K (UV light)	E_{def} (eV)	m (μ_B)
pristine BC_6N				1.228				0.00
pristine BC_6N-CO	−0.220	2.84	−0.012	1.226	5.35×10^{-9}	1.68×10^{-14}	0.14	0.00
pristine BC_6N-CO_2	−0.225	2.95	−0.015	1.221	6.37×10^{-9}	1.88×10^{-14}	0.23	0.00
pristine BC_6N-NO	−0.311	2.49	−0.071	0.000	1.84×10^{-9}	1.4×10^{-13}	0.15	0.96
pristine BC_6N-NO_2	−0.265	2.56	0.071	1.138	3.06×10^{-9}	4.79×10^{-14}	0.21	0.95
pristine BC_6N-NH_3	−0.264	3.27	−0.026	1.225	2.91×10^{-8}	4.27×10^{-14}	0.073	0.00
pristine BC_6N-H_2S	−0.260	2.40	0.044	1.222	2.54×10^{-8}	4.27×10^{-14}	0.15	0.00
pristine BC_6N-SO_2	−0.483	2.79	0.073	1.179	1.45×10^{-4}	7.69×10^{-12}	0.26	0.00
pristine BC_6N-H_2O	−0.258	2.88	−0.015	1.222	2.31×10^{-8}	4.07×10^{-14}	0.14	0.00
Pd-BC_6N		2.13		1.08				0.00
Pd-BC_6N-CO	−2.23	1.93	−0.207	1.116	5.13×10^{25}	3.68×10^6	0.071	0.00
Pd-BC_6N-CO_2	−0.64	2.15	0.046	1.070	7.87×10^{-2}	3.31×10^{-10}	−0.006	0.00
Pd-BC_6N-NO	−2.11	1.92	−0.127	0.000	5.77×10^{23}	2.51×10^5	0.13	0.84
Pd-BC_6N-NO_2	−1.82	2.12	0.175	0.000	6.34×10^{18}	2.7×10^2	0.036	0.94
Pd-BC_6N-NH_3	−1.61	2.20	−0.315	1.040	2.03×10^{15}	2.19	−0.004	0.00
Pd-BC_6N-H_2S	−1.67	2.38	−0.310	1.027	2.0×10^{16}	8.61	−0.003	0.00
Pd-BC_6N-SO_2	−1.28	2.38	−0.061	0.768	4.25×10^9	8.75×10^{-4}	0.107	0.00
Pd-BC_6N-H_2O	−1.14	2.28	−0.212	1.098	1.68×10^7	3.19×10^{-5}	0.06	0.00

$$E_{def} = E_{Pd/BC_6N+Molecule} - E^-_{Pd/BC_6N} \qquad (1)$$

where $E_{Pd/BC_6N + Molecule}$ and E^-_{Pd/BC_6N} are the total energies of the gas molecule with pristine BC_6N or the gas molecule-Pd-BC_6N complex and the pristine BC_6N or Pd-BC_6N sheet without a gas molecule (a molecule was removed from the optimized pristine BC_6N or gas molecule-Pd-BC_6N complex geometry, and total energy was computed), respectively. The E_{def} data are tabulated in Table 1. A comparison between deformation energies with adsorption energies obtained for gas molecules on the pristine BC_6N sheet shows that structural distortion plays a significant role for pristine BC_6N sheets.

The electronic band structures for all gases+pristine BC_6N sheets are plotted in Figure S1 (Supporting Information). The energy bandgaps for CO, CO_2, NH_3, H_2S, and H_2O-BC_6N were found to be 1.226, 1.221, 1.225, 1.222, and 1.222 eV, respectively. Hence, the electronic properties of pristine BC_6N were slightly changed upon interaction with CO, CO_2, NH_3, H_2S, and H_2O gas molecules (8 meV decrease in the pristine BC_6N energy bandgap). However, the adsorption of SO_2, NO, and NO_2 introduces one, three, and one flat impurity band inside the bandgap. As a result, the bandgap of the pristine BC_6N sheet drops 49 and 90 meV after interaction with SO_2 and NO_2, respectively. Interestingly, the NO-pristine BC_6N structure has a zero-energy bandgap, indicative of metallic behavior. The spin-polarized calculations showed that only adsorption of NO/NO_2 on pristine BC_6N induces a magnetic moment of 0.96/0.95 μB (see Table 1).

To get a better understanding of gas molecule adsorption on pristine BC_6N, the density of states (DOS) of the pristine BC_6N sheet along with different gas molecules is plotted in Figure S2 (Supporting Information). The disappearance of the DOS of CO, CO_2, NH_3, H_2S, and H_2O molecules around the Fermi level suggests that the gas molecules do not alter the electronic properties of BC_6N, supporting the weak interaction between them and the sheet. For SO_2-BC_6N, the presence of a peak attributed to SO_2 above the Fermi level results in a reduction of the pristine BC_6N energy bandgap. The NO

(NO_2) molecule contributes strongly at (around) the Fermi level, causing an electronic band dispersion around the Fermi level. These results agree well with the obtained electronic band structures. The detailed data of adsorption energies, the net charge transfer, the interaction distances, and the energy bandgap values for different systems are presented in Table 1.

As mentioned before, the low adsorption energies and the small charge transfer suggest that the interaction between molecules and pristine BC_6N is relatively weak, governed by vdW forces. In an attempt to improve the sensitivity of the BC_6N sheet, its surface was decorated by a metal atom (Pd). By trying different adsorption sites, it was revealed that the most favorable site for Pd is above the C atom with an atomic distance of 2.13 Å. The most stable configuration of Pd-decorated BC_6N alongside its band structure is shown in Figure 3a,b. The Pd adsorption energy on the BC_6N sheet was
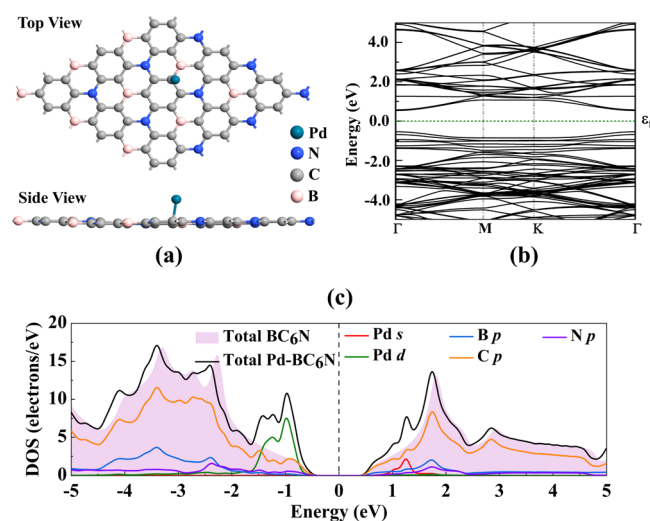
Figure 3. (a) Top and side view of the Pd-decorated BC_6N sheet. (b) Band structure plot of the Pd-decorated BC_6N sheet. (c) DOS plots for pristine BC_6N and Pd-decorated BC_6N sheets.
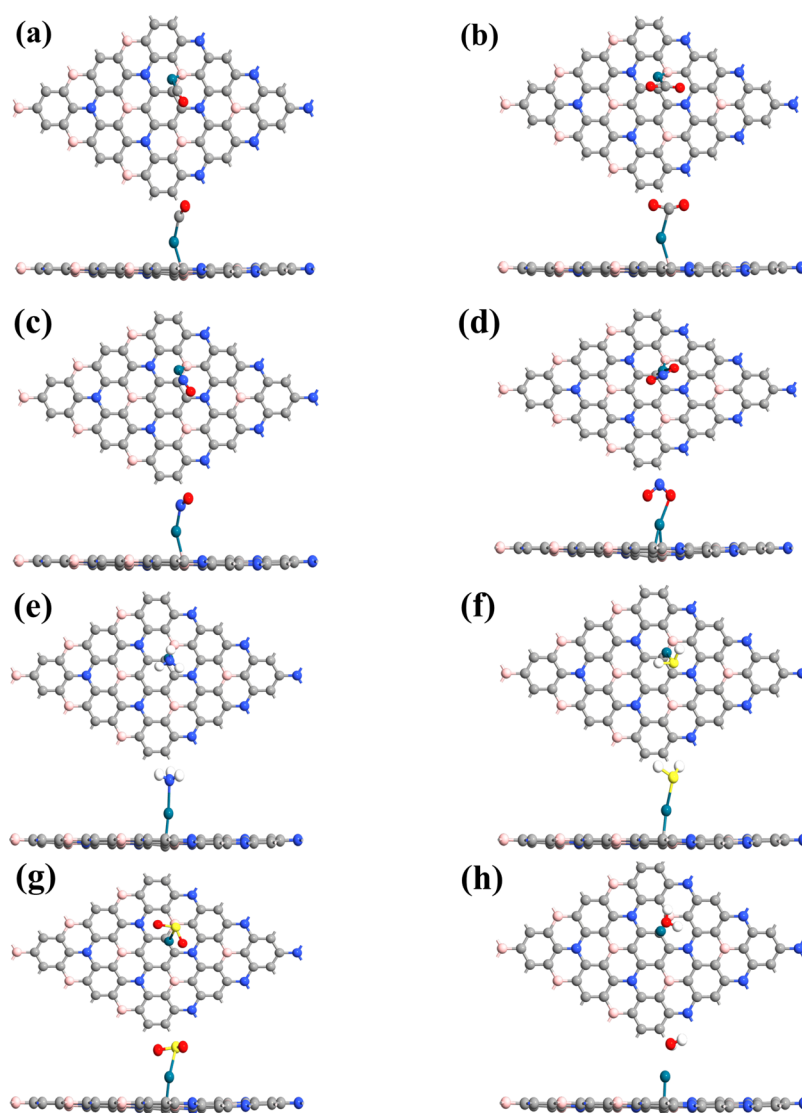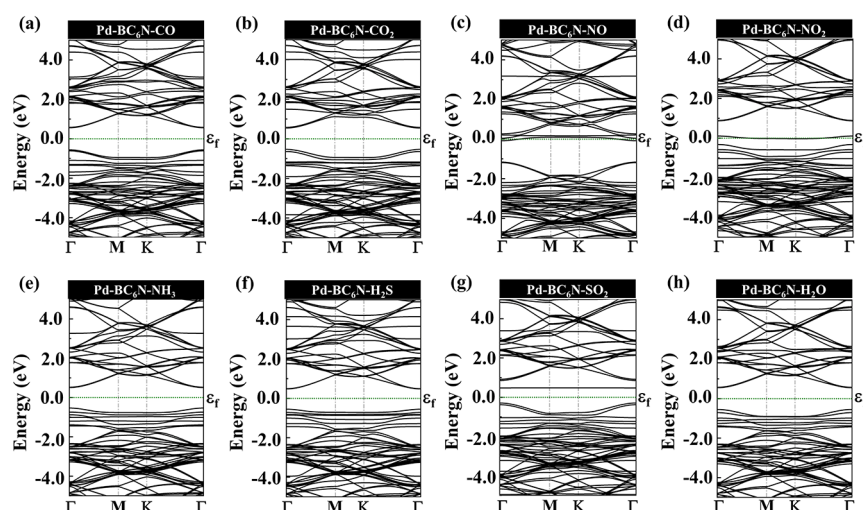
Figure 4. Most stable adsorption geometries of the Pd-decorated BC$_6$N sheet exposed to (a) CO, (b) CO$_2$, (c) NO, (d) NO$_2$, (e) NH$_3$, (f) H$_2$S, (g) SO$_2$, and (h) H$_2$O. Cyan, pink, gray, blue, red, yellow, and white balls represent Pd, B, C, N, O, S, and H atoms, respectively.

calculated to be −2.28 eV. As can be seen, the Pd-BC$_6$N sheet is a direct bandgap semiconductor (E_g = 1.080 eV). To examine the thermal stability of the Pd-BC$_6$N monolayer, AIMD simulation was performed at 300 K (Figure S3a (Supporting Information)). The total energy fluctuations in the order of 0.01 eV at 300 K without significant distortion confirm its thermal stability. The phonon spectrum was also examined in order to examine the dynamical stability of the Pd-BC$_6$N sheet (Figure S3b (Supporting Information)). The absence of imaginary frequencies (energies) implies dynamical stability.

Figure 3c compares the DOS curves of the Pd-decorated BC$_6$N sheet with the pristine BC$_6$N sheet. One can see that the bandgap of pristine BC$_6$N is reduced by 148 meV after decoration with a Pd atom, resulting in a conductivity enhancement of the system. Furthermore, new peaks emerged in DOS of BC$_6$N after decoration by Pd atoms at the energy range of −1.60 to −0.60 eV and 0.90 to 1.2 eV, attributed to the d and s orbitals of the metal atom, respectively. The electron configuration of Pd is [Kr] 4d.[10] The valence electrons attributed to the d orbital of a transition metal define the strength of the metal's bond. One can see that from

Figure 3c, the orbital hybridizations between the Pd d orbital and the C p orbital (in the valence band) and the Pd d orbital and the C s orbital (in the conduction band) confirm the existence of a covalent bond between Pd and C atoms. Besides that, the sum of atomic radii (2.36 Å) of Pd (1.69 Å) and C (0.67 Å) is larger than the Pd−C distance in the Pd-BC$_6$N sheet (2.13 Å), validating that the chemical bond is formed between Pd and C atoms.

The structures with the lowest energy after interaction of considered gas molecules with Pd-decorated BC$_6$N are depicted in Figure 4. It should be mentioned that the gas molecules were initially placed above the Pd atom with different orientations as discussed before for pristine BC$_6$N. For CO and NO molecules, they both adopted a parallel configuration with respect to Pd, where CO with an E_{ad} of −2.23 eV was tilted, and the C atom was bonded with Pd. Meanwhile, the N atom of NO was bonded with Pd with the same orientation as CO with an E_{ad} of −2.11 eV. The shortest distances of CO and NO gas molecules with Pd-BC$_6$N were estimated to be 1.93 Å (C−Pd) 1.92 Å (N−Pd), respectively. The CO$_2$ molecule was aligned parallel to BC$_6$N, and C was bonded with Pd with an E_{ad} of −0.64 eV. The shortest distance

Figure 5. Plots of electronic band structure for the Pd-decorated BC_6N sheet exposed to (a) CO, (b) CO_2, (c) NO, (d) NO_2, (e) NH_3, (f) H_2S, (g) SO_2, and (h) H_2O.

between CO_2 and Pd-BC_6N was 2.15 Å (C−Pd). NO_2 adopted a perpendicular orientation, where O was bonded to Pd with an E_{ad} of −1.82 eV, and the shortest distance between the O atom of NO_2 and Pd was 2.12 Å (O−Pd). NH_3 preferred a parallel orientation with an E_{ad} of −1.61 eV and the shortest distance of 2.20 Å (N−Pd). H_2S was orientated perpendicular with respect to BC_6N with the shortest distance of 2.38 Å (S−Pd) and an E_{ad} of −1.67. SO_2 adopted a parallel orientation regarding the BC_6N surface with an E_{ad} of −1.28 eV, and the shortest distance between the S atom of SO_2 and Pd was 2.38 Å. Despite all other molecules, H_2O was not bonded with Pd with an E_{ad} of −1.14 eV and adopted a parallel orientation with the shortest distance of 2.28 Å (O−Pd). It is worth mentioning that for CO, NO, and CO_2 adsorption configurations, Pd was bonded with the B atom of BC_6N after optimization with the binding distances of 2.29, 2.29, and 2.30 Å, respectively. Moreover, Pd was bonded with both C and B atoms of BC_6N after interaction with NO_2 with binding distances of 2.21 and 2.23 Å, respectively. However, Pd remained in the same position and bonded to the C atom of BC_6N after interaction with NH_3, H_2S, SO_2, and H_2O molecules with the binding distances of 2.13, 2.21, 2.16, and 2.11 Å, respectively. According to our calculations, there is a net charge of 0.207, 0.127, 0.315, 0.31, 0.061, and 0.212 e, donated from CO, NO, NH_3, H_2S, SO_2, and H_2O, respectively, to the Pd atom. On the other hand, the net charges of 0.046 and 0.175 e were transferred from Pd to CO_2 and NO_2, respectively. Based on eq 1, the deformation energies for the Pd-BC_6N sheet after interaction with gas molecules were also calculated. The detailed data of deformation energies and adsorption energies with the binding distances and charge transfer for different adsorption configurations of molecule-Pd-BC_6N are provided in Table 1. The deformation energies for these Pd-BC_6N samples after interaction with molecules were found to be between 0.003 and 0.13 eV. The smaller values of deformation energies for Pd-BC_6N compared to pristine BC_6N can be attributed to the presence of the Pd atom. While the surface of the BC_6N sheet was distorted in the interaction area upon adsorption of the molecules, in the case of Pd-BC_6N, the Pd atom as a capturing center interacts with the molecules, causing the Pd−C bond to get distorted. Table S1 (Supporting Information) lists the Pd−C bond lengths before and after

interaction with gas molecules. It is clear that the Pd−C bond length was decreased in almost all cases due to the interaction between the gas molecule and the Pd atom. It is worth mentioning that C−C, C−B, and C−N bonds are somewhat augmented upon the interaction of the gas molecules with Pd-BC_6N because of the deterioration of the strength of the Pd−C bond.

To have a better understanding of the adsorption behaviors of molecules on Pd-BC_6N, their electronic band structures are provided in Figure 5. The energy bandgaps for CO-, CO_2-, NH_3, H_2S-, SO_2-, and H_2O-Pd-BC_6N obtained were 1.116, 1.07, 1.04, 1.027, 0.768, and 1.098 eV, respectively. In other words, the energy bandgap of Pd-BC_6N changes by 36, 10, 40, 53, and 18 meV after interaction with CO, CO_2, NH_3, H_2S, and H_2O, respectively, indicating that the molecule adsorption yields trivial effects on the band structure near the Fermi level. For SO_2 adsorption, the energy bandgap of Pd-BC_6N reduces to 0.768 eV (312 meV change). The electronic properties of Pd-BC_6N undergo significant changes after NO and NO_2 adsorption. The energy bandgaps of NO- and NO_2-Pd-BC_6N were found to be zero, suggesting metallic behavior. The decoration of BC_6N with Pd does not result in spin polarization. The NO and NO_2 gas molecules cause a magnetic moment of 0.84 and 0.94 μB in Pd-decorated BC_6N, respectively, which are slightly less than those obtained for pristine BC_6N.

The projected DOS (PDOS) of the molecules on Pd-BC_6N is presented in Figure 6 to help shed light on the adsorption mechanism. When the gas molecules and the Pd atom interact, orbital hybridization between Pd 4d and the s and p orbitals of the gas molecules happens, meaning that the PDOS of two orbitals appears in the same energy. For CO, CO_2, NH_3, H_2S, and H_2O-Pd-BC_6N, no overlapping peaks were observed near the Fermi level, suggesting no significant bandgap change caused by gas molecule adsorption. However, the hybridization of the Pd d orbital and the p orbital of N in NO (O in NO_2) can be confirmed owing to the overlapping peaks in their PDOS. In comparison with pristine BC_6N, the DOS of Pd-decorated BC_6N for NO (NO_2) displays a large peak above (at) the Fermi level, implicating a substantial change in electronic properties of the Pd-BC_6N sensor and a semi-conductor−metal transition. The large peaks around the Fermi
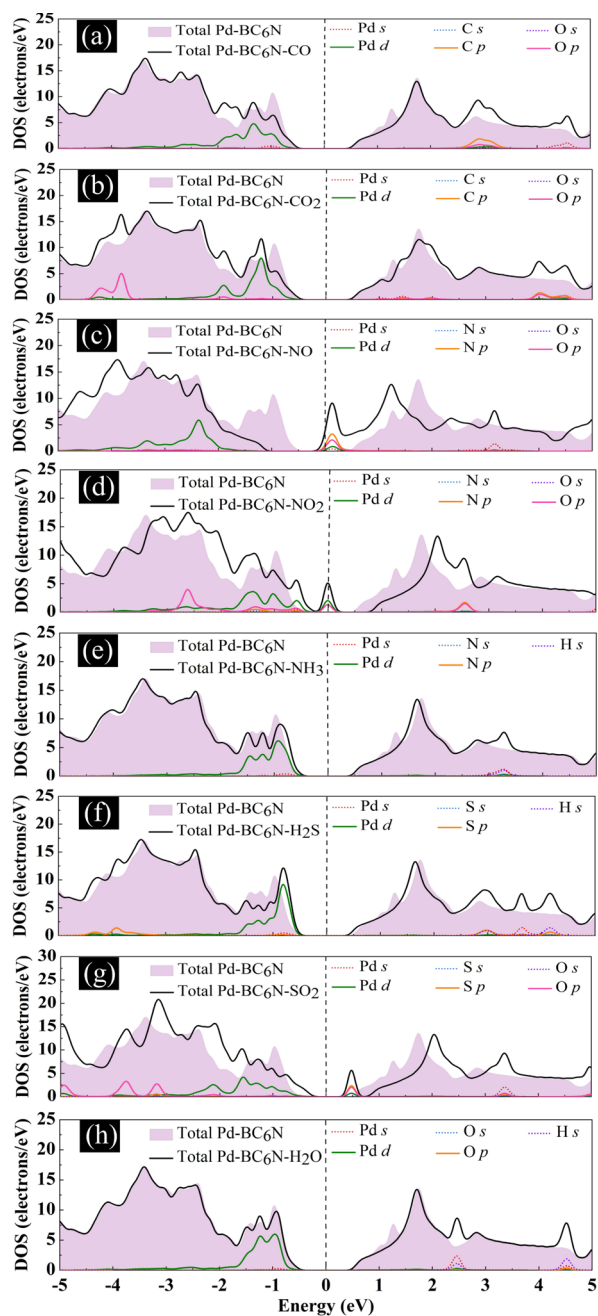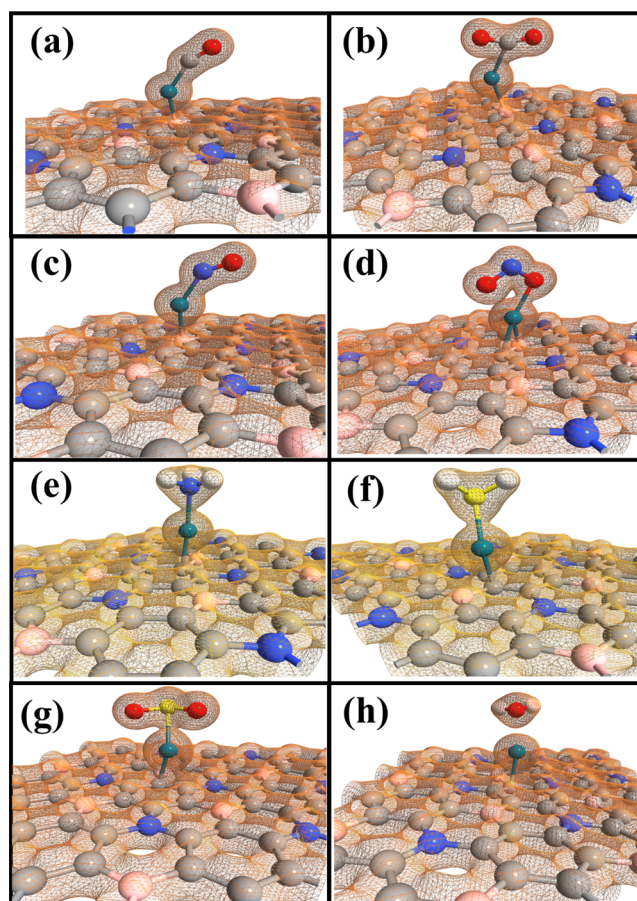
Figure 6. DOS plots for the Pd-decorated BC_6N sheet exposed to (a) CO, (b) CO_2, (c) NO, (d) NO_2, (e) NH_3, (f) H_2S, (g) SO_2, and (h) H_2O.

Figure 7. Electronic total charge densities for the Pd-decorated BC_6N sheet exposed to (a) CO, (b) CO_2, (c) NO, (d) NO_2, (e) NH_3, (f) H_2S, (g) SO_2, and (h) H_2O. Pd, cyan; B, pink; C, gray; N, blue; O, red; S, yellow; H, white.

level indicate that the conductivity of the Pd-BC_6N system is significantly increased because of NO or NO_2 adsorption. These findings agree well with the electronic band structure results. In the case of Pd-BC_6N-SO_2, an overlapping peak was found at +0.5 eV caused by Pd d orbital and S p orbital hybridization. This sharp peak is attributed to the flat band in the Pd-BC_6N-SO_2 band structure.

Furthermore, the electron density of Pd-decorated BC_6N toward different gas molecules is displayed in Figure 7. An orbital overlap can be observed between CO, NO, CO_2, NO_2, NH_3, H_2S, and SO_2 gas molecules and the Pd atom, showing the existence of chemisorption. The atomic radii are 0.87, 0.67, 0.56, 1.69, 0.48, 0.88, and 0.53 Å for B, C, N, Pd, O, S, and H atoms, respectively.[34] According to Table 1, the minimum

distances between Pd and CO (Pd−C), CO_2 (Pd−C), NO (Pd−N), NO_2 (Pd−O), NH_3 (Pd−N), H_2S (Pd−S), SO_2 (Pd−S), and H_2O (Pd−O) are 1.93, 2.15, 1.92, 2.12, 2.20, 2.38, 2.38, and 2.28 Å, respectively, while the sums of corresponding atomic radii are 2.36, 2.36, 2.25, 2.17, 2.25, 2.57, 2.57, and 2.22 Å, respectively. It can be deduced that the minimum distance between the Pd atom and the atom in all gas molecules except H_2O is less than the sums of corresponding atomic radii, suggestive of a covalent bond between Pd and the gas molecules. Hence, the water molecule is only physisorbed on the surface.

To assess and analyze the performance of a gas sensor, three important indicators should be considered, including recovery time, sensitivity, and selectivity. To achieve a gas sensor with high performance, short recovery time, high sensitivity, and selectivity are required. From conventional transition state theory, the recovery time (τ) of a sensor, which is the time taken for the target gas to be desorbed from the surface, is[37]

$$\tau = v_0^{-1} \exp(-E_{ad}/k_B T) \qquad (2)$$

Here, T is the temperature, and k_B is the Boltzmann constant. v_0 is the attempt frequency, which is the vibration frequency of single bonds between the molecule and the surface. This frequency is related to the chemical reactions, which can be described with transition state theory and collision theory.[38] Considering the transition state theory, the attempt frequency

can be assumed constant. Nevertheless, when taking into account collision theory, space or volume is an underlying factor that can affect the frequency of collision for a given molecule. Here, for simplification purposes, the attempt frequency was considered constant. The values of the recovery time of the systems are listed in Table 1. In visible light ($v_0 = 10^{12}$ Hz) and at room temperature ($T = 298$ K), the τ values for pristine BC_6N structures were achieved, 5.35×10^{-9}, 6.37×10^{-9}, 1.84×10^{-9}, 3.06×10^{-9}, 2.91×10^{-8}, 2.54×10^{-8}, 1.45×10^{-4}, and 2.31×10^{-8} s, for CO, CO_2, NO, NO_2, NH_3, H_2S, SO_2, and H_2O adsorption, respectively. It is worth mentioning that the nanosecond recovery time is too short for realizing detection in a real experiment because the sensor cannot hold the gas molecules. This is attributed to the small obtained adsorption energies for the gas molecule-pristine BC_6N sheet. As a result, pristine BC_6N cannot be considered as an option for the detection of the above gases.

For Pd-decorated BC_6N structures, the τ values at room temperature under visible light were 5.13×10^{25}, 7.87×10^{-2}, 5.77×10^{23}, 6.34×10^{18}, 2.03×10^{15}, 2.0×10^{16}, 4.25×10^9, and 1.68×10^7 s, for CO, CO_2, NO, NO_2, NH_3, H_2S, SO_2, and H_2O, respectively. As expected, a short full recovery was not attained because of the high adsorption energies of gas molecules on Pd-BC_6N. Based on eq 2, increasing the temperature and the attempt frequency at constant adsorption energy will reduce the recovery time. It was reported that ultraviolet (UV) radiation facilitates the sensor's recovery by reducing the desorption barrier.[39] Therefore, a combination of UV illumination and annealing treatment was used to improve the recovery process. The recovery time for considered structures at 298, 398, and 498 K under visible and UV light has been calculated (see Table S2 (Supporting Information)). It was found that a combination of UV exposure and annealing at 498 K results in a reasonable recovery time for the Pd-BC_6N sensor. The achieved τ values, for adsorption of CO, CO_2, NO, NO_2, NH_3, H_2S, SO_2, and H_2O from the Pd-BC_6N sheet at a temperature of 498 K under UV exposure ($v_0 = 10^{15}$ Hz), were found to be 3.68×10^6, 3.31×10^{-10}, 2.51×10^5, 2.7×10^2, 2.19, 8.61, 8.75×10^{-4}, and 3.19×10^{-5} s, respectively.

Next, in order to track the conductance change, transport calculations in terms of the $I-V$ characteristics of the sensors were obtained. Since the structure of BC_6N is anisotropic, the electronic transport study was calculated along with both armchair and zigzag directions, as shown in Figure 8. The left and right electrodes were assumed to be periodic in x and y directions and were connected to the central region in the z-direction (transport direction). The electrode sizes for armchair (zigzag) directions were selected to be 14.76 Å × 8.52 Å (17.05 Å × 4.92 Å). Additionally, the sizes of the central region for armchair and zigzag were selected to be 14.76 Å × 25.57 Å and 17.05 Å × 14.76 Å, respectively.

When bias voltage in excess of the threshold voltage is applied to the sensor, the valence band maximum (VBM) of the left electrode meets the conduction band minimum (CBM) of the right electrode, and the device allows current to flow. From Figure 8, no current passed through the device until the bias voltage surmounts 1.2 V. By introducing the gas molecules in the central region, except for NO and NO_2, no significant change was observed in the current transport through pristine or Pd-decorated BC_6N, indicative of low sensitivity of the sensor toward the CO, CO_2, NH_3, SO_2, H_2S, and H_2O molecules. To get a better sense of the changes in the $I-V$ curves of the sensors after gas adsorption, the sensor's
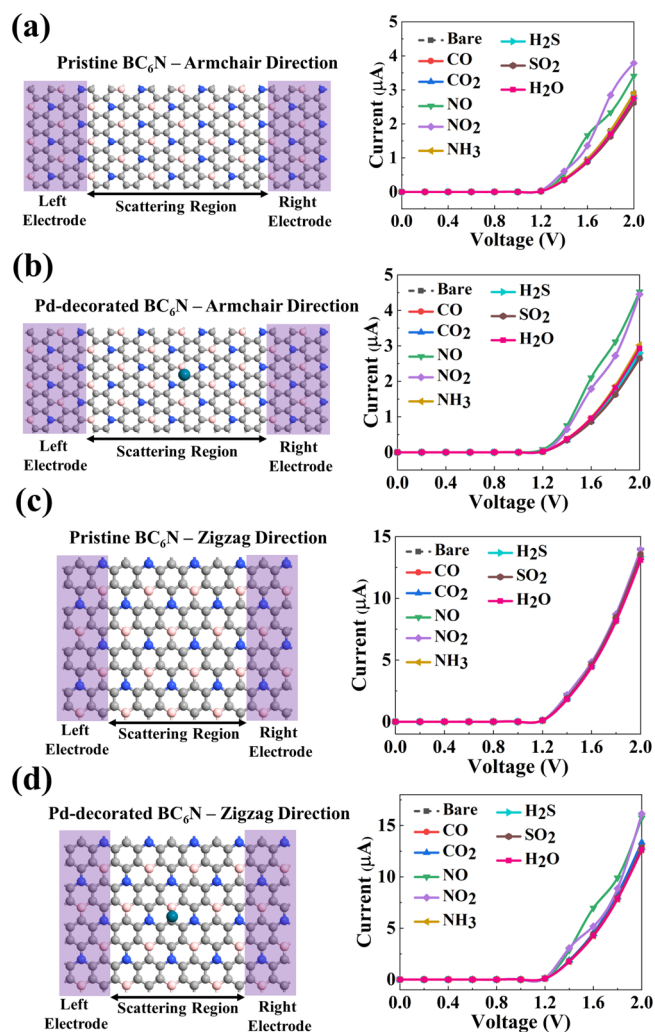

Figure 8. Transport model and current–voltage characteristics for armchair and zigzag directions. (a) Pristine BC_6N–armchair direction. (b) Pd-decorated BC_6N–armchair direction. (c) Pristine BC_6N–zigzag direction. (d) Pd-decorated BC_6N–zigzag direction. B, pink; C, gray; N, blue; Pd, cyan.

sensitivity was calculated. Sensitivity, the variation in conductance, can be expressed as follows

$$S = \left| \frac{G_{gas} - G_{pure}}{G_{pure}} \right| \times 100 \tag{3}$$

Here, G_{gas} and G_{pure} are the conductivity of a gas molecule-adsorbed BC_6N sheet and an isolated BC_6N sheet (Pd-BC_6N sheet), respectively. From Figure 8, first, the conductance (I/V) for different configurations was obtained, and then, the sensitivity for both armchair and zigzag directions (including pristine and Pd-decorated BC_6N) at bias voltages of 1.4, 1.6, 1.8, and 2.0 V was calculated. Figure 9a,b compares the sensitivity of pristine and Pd-decorated structures in the armchair direction at a bias voltage of 1.6 V and the zigzag direction at a bias voltage of 1.4 V. At 1.6 V in the armchair direction (Figure 9a), 73.6 and 42.1% sensitivities were observed for sensing NO and NO_2 gas molecules by the pristine structure, respectively. In addition, at the same voltage, for Pd-decorated BC_6N, sensitivities of 134 and 98.6% were achieved for NO and NO_2, respectively. Similarly, at 1.4 V in the zigzag direction (Figure 9b), sensitivities of 16.4 and 16.9%
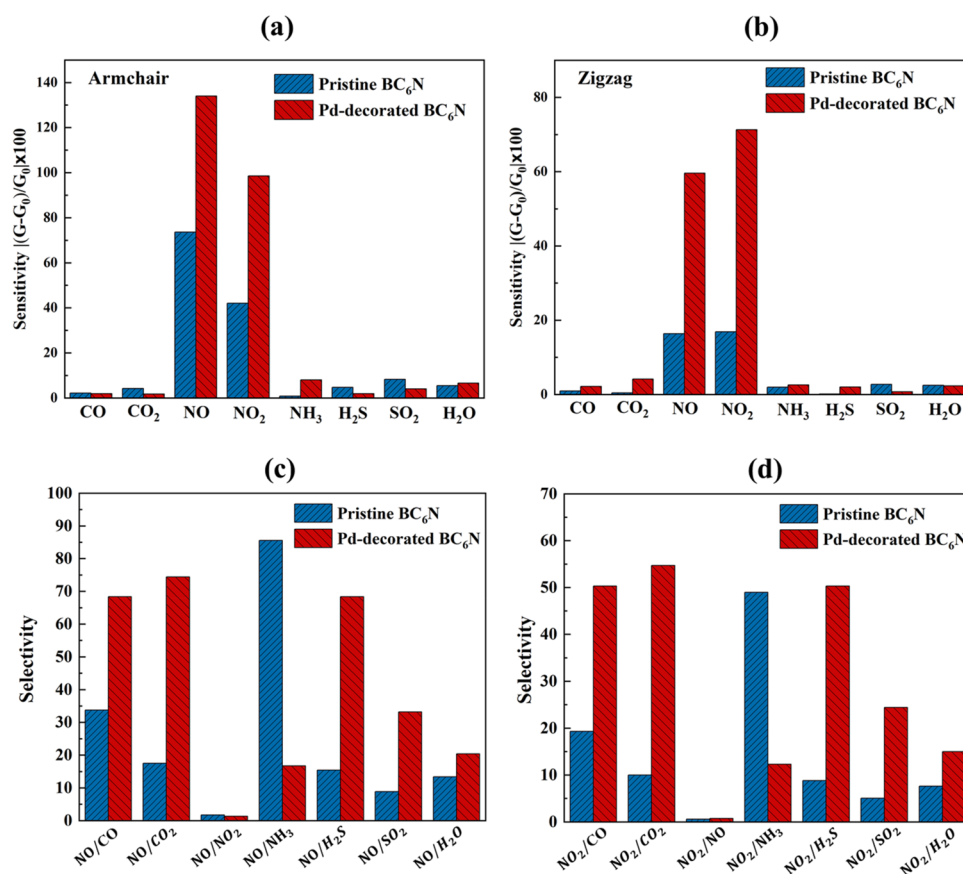
Figure 9. Sensitivity for the pristine and Pd-decorated BC_6N sheet with adsorbed CO, CO_2, NO, NO_2, NH_3, H_2S, SO_2, and H_2O for (a) armchair and (b) zigzag directions. Selectivity of (c) NO and (d) NO_2 over other considered gas molecules for pristine and Pd-decorated BC_6N sheets.

were obtained for the pristine structure for sensing NO and NO_2, respectively. Although, at the same voltage, for Pd-decorated BC_6N, sensitivities of 59.6 and 71.3% were achieved for sensing NO and NO_2, respectively. It is evident that the sensitivity of BC_6N toward NO_x gas molecules has been improved by Pd decoration.

From Figure 8, highly anisotropic I−V responses along with armchair and zigzag directions can be observed. The current decreased from the zigzag to armchair direction at the scale of ∼10 μA at a 2 V bias voltage after gas exposure. The anisotropic transport properties of BC_6N originated from its anisotropic electronic band structure. As can be seen in Figure S4 (Supporting Information), both the valence band maximum (VBM) and the conduction band minimum (CBM) are notably dispersed along the Γ−K direction (reciprocal space), which is the zigzag direction in real space. However, along the Γ−M direction (reciprocal space), which is the armchair direction in real space, the VBM and CBM are nearly flat. Since the effective mass is proportional to the inverse of the curvature of the band dispersion, the zigzag direction with flat bands shows a higher current. Ergo, the results of the I−V profiles of Pd-BC_6N under gas exposure become remarkably differentiable along the armchair direction as compared with those along the zigzag.

To quantify the selectivity of considered molecules, a comparative analysis was done. For this purpose, the ratios of the sensitivity of NO and NO_2 to other gases were calculated and are shown in Figure 9c,d. Since the values of sensitivity for NO_x in the armchair direction are higher than those in the zigzag direction, here, we reported the selectivity in the

armchair direction. The sensitivity ratios of NO (NO_2) to CO, CO_2, NH_3, H_2S, SO_2, and H_2O for the Pd-decorated BC_6N sheet as a channel material were found to be 68.4 (50.3), 74.4 (54.7), 16.7 (12.3), 68.4 (50.3), 33.2 (24.4), and 20.4 (15), respectively, implying that NO_x selective detection can be accomplished. Except for NH_3, Pd-BC_6N offered a better selectivity for NO_x detection in comparison with pristine BC_6N.

Table S3 (Supporting Information) compares the adsorption energy and the performance of the 2D-based sensors for the detection of inorganic and sulfur-based gas molecules. One can notice stronger interactions between the gas molecules and the Pd-decorated BC_6N sheet in comparison with 2D materials such as graphene,[40] germanene,[41] phosphorene,[42] MoS_2,[43] silicene,[44] borophene,[45] BC_3,[46] etc. The performance of gas sensors for most of the 2D materials was not reported. For BC_3, the interaction of CO and NH_3 on the BC_3 surface caused 4.63 and 16.7% variations for the bandgap, respectively.[46] Therefore, the Pd-BC_6N-based sensor performs very well regarding its sensitivity and selectivity, which surpasses many 2D sensors.

In summary, in order to produce an efficient sensor, the adsorption should be strong enough to keep the analytes on the sensing material's surface and weak enough to allow the analytes to be dislodged from the surface without ruining it. Although pristine BC_6N shows a decent sensitivity and selectivity for NO_x detection, the nanosecond recovery time and low adsorption energy limit its gas sensing applications because the sensor cannot hold the gas species for an accurate conductance measurement in a real experiment. To overcome

the limitations of pristine BC_6N, in the past, we investigated defective BC_6N[47] in VOC gases, and here, we have investigated metal-decorated BC_6N in inorganic and sulfur-containing gases. Our results show that Pd-BC_6N exhibited excellent sensitivity (98.6−134%) and high selectivity (12.3−74.4 times) toward NO_x gas molecules accompanied by large adsorption energies. We found that both armchair and zigzag configurations of pristine and Pd-BC_6N show high sensitivity and selectivity to NO_x gas molecules. We also disclosed that the Pd-decorated BC_6N sensor could recover in 270 s under UV radiation at 400 K. Furthermore, our findings demonstrate that the gas sensing performance's judgment only from calculated adsorption energy would not have led to a reliable prediction. Despite the fact that the adsorption energy of CO (−2.23 eV) is higher than that of NO (−2.11 eV) on Pd-decorated BC_6N, it can be seen that the sensor can detect NO with much higher sensitivity compared to CO (selectivity of 68.4). Interestingly, our proposed sensor showed low sensitivity toward H_2O and CO_2 (as interfering molecules in breath); therefore, the sensor performance for the detection of target biomarkers was not affected by humidity. The presence of NO_x in human breath above 50 ppb could be indicative of cardiovascular diseases and respiratory (pulmonary) inflammation.[48] Hence, Pd-decorated BC_6N could be a very encouraging 2D material for analyzing pulmonary disease and cardiovascular biomarkers, among other ailments of the stomach, kidney, and intestine.

CONCLUSION

In this study, we scrutinized the adsorption behavior of several gases (NO, NO_2, NH_3, CO, CO_2, H_2S, and SO_2) as disease biomarkers as wells as H_2O as an interfering gas from human breath on the pristine and Pd-decorated BC_6N sheets using first-principles DFT calculations and the NEGF method. It was disclosed that the gas molecule adsorption on the pristine BC_6N sheet involved physisorption owing to small adsorption energies. It was revealed that the decoration of BC_6N with Pd increases the adsorption energies considerably, resulting in chemisorption. The I−V characteristics showed that the sensor based on Pd-decorated BC_6N is highly sensitive (98.6−134%) and selective (12.3−74.4 times) toward NO_x gas molecules and insensitive to humidity and CO_2. Furthermore, the reusability of the sensor was evaluated by the recovery time, and it was observed that the sensor has a short recovery time under UV radiation at 498 K. Overall, Pd-decorated BC_6N was introduced as a promising 2D material for analyzing human breath for disease diagnosis applications.

METHODS

DFT calculations combined with NEGF, as executed in the Atomistix ToolKit package (ATK), were carried out in this paper.[49] The exchange and correlation functionals were treated by generalized gradient approximation (GGA) of Perdew−Burke−Ernzerhof (PBE). The Fritz Haber Institute (FHI) pseudopotentials with a double-zeta basis set were utilized. The cutoff energy was set to be 800 eV for the plane-wave basis. A sufficiently large vacuum space of 20 Å was considered to eradicate the image−image interactions. The van der Waals (vdW) interactions were included using the D2 method of Grimme.[50] The limited-memory Broyden−Fletcher−Gold-farb−Shanno (LBFGS) quasi-Newton method was employed to fully optimize the structures until the force on each atom

was smaller than 0.01 eV/Å. For the primitive Brillouin zones, sampling was executed with $3 \times 3 \times 1$ k-points for optimization and was then increased to $5 \times 5 \times 1$ k-points for electronic calculations.

The adsorption energy of gas molecules on the pristine BC_6N sheet or the Pd-decorated BC_6N sheet was calculated by

$$E_{ad} = E_{Pd/BC_6N+Molecule} - (E_{Pd/BC_6N} + E_{Molecule}) \qquad (4)$$

where $E_{Pd/BC_6N + Molecule}$, E_{Pd/BC_6N}, and $E_{Molecule}$ are the total energies of the gas molecule-pristine BC_6N or gas molecule-Pd-BC_6N complex, the pristine BC_6N or Pd-BC_6N sheet, and the isolated gas molecule, respectively. Besides that, the charge transfer (Q_T) after the interaction of the analytes with the sensing material was calculated using Mulliken population analysis.

DFT in combination with the NEGF technique was used for the electron transport calculation of the BC_6N devices. In the device configuration, the metal electrodes were connected to the central region in the z-direction (the transport direction). Under a finite bias voltage (V_b), the electrical current passed through the device was calculated by the Landauer−Büttiker formula[51,52]

$$I = \frac{2e}{h} \int_{\mu_L}^{\mu_R} T(E, V_b)[f_R(E, V_b) - f_L(E, V_b)]dE \qquad (5)$$

Here, T and f are the energy (E) and bias voltage-dependent transmission function and the Fermi−Dirac distribution function, respectively. $\mu_{R(L)} = E_f \pm eV_b/2$ is the chemical potential of the right (left) electrodes, where E_f is the Fermi energy. For electron transport calculations, $1 \times 3 \times 50$ Monkhorst−Pack k-points for sampling the Brillouin zone were chosen.

In order to evaluate the thermal stability of the structures, ab initio molecular dynamics (AIMD) simulation at 300 K (Nosé−Hoover thermostat) for 10 ps with a time step of 1 fs was performed. Dynamical stability at 300 K was also investigated using phonon band structure calculations by adopting GGA-PBE-FHI.

ASSOCIATED CONTENT

Supporting Information

The Supporting Information is available free of charge at https://pubs.acs.org/doi/10.1021/acsomega.0c05495.

(Table S1) Minimum distance, (Table S2) recovery time (τ) in different conditions in s, (Table S3) review of 2D material-based gas sensors, (Figure S1a−h) plots of electronic band structure for the pristine BC_6N sheet, (Figure S2a−h) DOS plots for the pristine BC_6N sheet, (Figure S3a,b) thermal and dynamical stability of Pd-decorated BC_6N at 300 K, and (Figure S4a,b) highly anisotropic BC_6N (PDF)

AUTHOR INFORMATION

Corresponding Authors

Sadegh Mehdi Aghaei − *Small Systems Laboratory, Department of Mechanical Engineering, Worcester Polytechnic Institute, Worcester, Massachusetts 01609, United States;* ⓘ orcid.org/0000-0002-0108-8994; Email: smaghaei@wpi.edu

Balaji Panchapakesan − *Small Systems Laboratory, Department of Mechanical Engineering, Worcester*

Polytechnic Institute, Worcester, Massachusetts 01609, United States; ⓞ orcid.org/0000-0002-0860-3602; Email: bpanchapakesan@wpi.edu

Author

Aref Aasi − *Small Systems Laboratory, Department of Mechanical Engineering, Worcester Polytechnic Institute, Worcester, Massachusetts 01609, United States;* ⓞ orcid.org/0000-0002-5485-2503

Complete contact information is available at:
https://pubs.acs.org/10.1021/acsomega.0c05495

■ **ACKNOWLEDGMENTS**

■ **REFERENCES**

(1) Novoselov, K. S.; Geim, A. K.; Morozov, S. V.; Jiang, D.; Zhang, Y.; Dubonos, S. V.; Grigorieva, I. V.; Firsov, A. A. Electric field effect in atomically thin carbon films. *Science* **2004**, *306*, 666−669.

(2) Choi, W.; Lahiri, I.; Seelaboyina, R.; Kang, Y. S. Synthesis of graphene and its applications: a review. *Crit. Rev. Solid State Mater. Sci.* **2010**, *35*, 52−71.

(3) Geim, A. K.; Novoselov, K. S. The rise of graphene. *Nat. Mater.* **2007**, *6*, 183−191.

(4) Jadoon, T.; Carter-Fenk, K.; Siddique, M. B. A.; Herbert, J. M.; Hussain, R.; Iqbal, S.; Iqbal, J.; Ayub, K. Silver clusters tune up electronic properties of graphene nanoflakes: A comprehensive theoretical study. *J. Mol. Liq.* **2020**, *297*, 111902.

(5) Hussain, R.; Saeed, M.; Mehboob, M. Y.; Khan, S. U.; Khan, M. U.; Adnan, M.; Ahmed, M.; Iqbal, J.; Ayub, K. Density functional theory study of palladium cluster adsorption on a graphene support. *RSC Adv.* **2020**, *10*, 20595−20607.

(6) Ganji, M. D.; Sharifi, N.; Ardjmand, M.; Ahangari, M. G. Pt-decorated graphene as superior media for H_2S adsorption: a first-principles study. *Appl. Surf. Sci.* **2012**, *261*, 697−704.

(7) Rad, A. S.; Abedini, E. Chemisorption of NO on Pt-decorated graphene as modified nanostructure media: a first principles study. *Appl. Surf. Sci.* **2016**, *360*, 1041−1046.

(8) Bo, Z.; Guo, X.; Wei, X.; Yang, H.; Yan, J.; Cen, K. Density functional theory calculations of NO_2 and H_2S adsorption on the group 10 transition metal (Ni, Pd and Pt) decorated graphene. *Phys. E* **2019**, *109*, 156−163.

(9) Radisavljevic, B.; Radenovic, A.; Brivio, J.; Giacometti, V.; Kis, A. Single-layer MoS_2 transistors. *Nat. Nanotechnol.* **2011**, *6*, 147−150.

(10) Jo, S.; Ubrig, N.; Berger, H.; Kuzmenko, A. B.; Morpurgo, A. F. Mono- and bilayer WS_2 light-emitting transistors. *Nano Lett.* **2014**, *14*, 2019−2025.

(11) Li, L.; Yu, Y.; Ye, G. J.; Ge, Q.; Ou, X.; Wu, H.; Feng, D.; Chen, X. H.; Zhang, Y. Black phosphorus field-effect transistors. *Nat. Nanotechnol.* **2014**, *9*, 372.

(12) Wang, X.; Li, X.; Zhang, L.; Yoon, Y.; Weber, P. K.; Wang, H.; Guo, J.; Dai, H. N-doping of graphene through electrothermal reactions with ammonia. *Science* **2009**, *324*, 768−771.

(13) Martins, T. B.; Miwa, R. H.; da Silva, A. J. R.; Fazzio, A. Electronic and transport properties of boron-doped graphene nanoribbons. *Phys. Rev. Lett.* **2007**, *98*, 196803.

(14) Rahaman, O.; Mortazavi, B.; Dianat, A.; Cuniberti, G.; Rabczuk, T. A structural insight into mechanical strength of graphene-like carbon and carbon nitride networks. *Nanotechnology* **2016**, *28*, No. 055707.

(15) Rao, C. N. R.; Pramoda, K. Borocarbonitrides, $B_xC_yN_z$, 2D nanocomposites with novel properties. *Bull. Chem. Soc. Jpn.* **2019**, *92*, 441−468.

(16) Matsui, K.; Oda, S.; Yoshiura, K.; Nakajima, K.; Yasuda, N.; Hatakeyama, T. One-shot multiple borylation toward BN-doped nanographenes. *J. Am. Chem. Soc.* **2018**, *140*, 1195−1198.

(17) Liu, X.; Ma, X.; Gao, H.; Zhang, X.; Ai, H.; Li, W.; Zhao, M. Valley-selective circular dichroism and high carrier mobility of graphene-like BC_6N. *Nanoscale* **2018**, *10*, 13179−13186.

(18) Mortazavi, B.; Shahrokhi, M.; Raeisi, M.; Zhuang, X.; Pereira, L. F. C.; Rabczuk, T. Outstanding strength, optical characteristics and thermal conductivity of graphene-like BC_3 and BC_6N semiconductors. *Carbon* **2019**, *149*, 733−742.

(19) Kaneko, T.; Harigaya, K. Dependence of Atomic Arrangement on Length of Flat Bands in Zigzag BC_2N Nanoribbons. *J. Phys. Soc. Jpn.* **2013**, *82*, No. 044708.

(20) Shi, L.-B.; Yang, M.; Cao, S.; You, Q.; Zhang, Y.-J.; Qi, M.; Zhang, K.-C.; Qian, P. Prediction of high carrier mobility for a novel two-dimensional semiconductor of BC_6N: first principles calculations. *J. Mater. Chem. C* **2020**, *8*, 5882−5893.

(21) Ryter, S. W.; Morse, D.; Choi, A. M. K. Carbon monoxide: to boldly go where NO has gone before. *Science Signaling* **2004**, *2004*, re6−re6.

(22) Oakley-Girvan, I.; Davis, S. W. Breath based volatile organic compounds in the detection of breast, lung, and colorectal cancers: A systematic review. *Cancer Biomarkers* **2018**, *21*, 29−39.

(23) Ellis, J. E.; Star, A. Carbon nanotube based gas sensors toward breath analysis. *ChemPlusChem* **2016**, *81*, 1248.

(24) Tripathi, K. M.; Kim, T.; Losic, D.; Tung, T. T. Recent advances in engineered graphene and composites for detection of volatile organic compounds (VOCs) and non-invasive diseases diagnosis. *Carbon* **2016**, *110*, 97−129.

(25) Aasi, A.; Aghaei, S. M.; Panchapakesan, B. A density functional theory study on the interaction of toluene with transition metal decorated carbon nanotubes: a promising platform for early detection of lung cancer from human breath. *Nanotechnology* **2020**, *31*, 415707.

(26) Aasi, A.; Aghaei, S. M.; Moore, M. D.; Panchapakesan, B. Pt-, Rh-, Ru-, and Cu-Single-Wall Carbon Nanotubes Are Exceptional Candidates for Design of Anti-Viral Surfaces: A Theoretical Study. *Int. J. Mol. Sci.* **2020**, *21*, 5211.

(27) Balandin, A. A.; Ghosh, S.; Bao, W.; Calizo, I.; Teweldebrhan, D.; Miao, F.; Lau, C. N. Superior thermal conductivity of single-layer graphene. *Nano Lett.* **2008**, *8*, 902−907.

(28) Peyghan, A. A.; Yourdkhani, S.; Noei, M. Working mechanism of a BC_3nanotube carbon monoxide gas sensor. *Commun. Theor. Phys.* **2013**, *60*, 113.

(29) Ma, D.; Zhang, J.; Li, X.; He, C.; Lu, Z.; Lu, Z.; Yang, Z.; Wang, Y. C_3N monolayers as promising candidates for NO_2 sensors. *Sens. Actuators B Chem.* **2018**, *266*, 664−673.

(30) Beheshtian, J.; Peyghan, A. A.; Noei, M. Sensing behavior of Al and Si doped BC_3 graphenes to formaldehyde. *Sens. Actuators B Chem.* **2013**, *181*, 829−834.

(31) Bafekry, A. Graphene-like BC_6N single-layer: Tunable electronic and magnetic properties via thickness, gating, topological defects, and adatom/molecule. *Physica E Low Dimens. Syst. Nanostruct.* **2020**, *118*, 113850.

(32) Babar, V.; Sharma, S.; Schwingenschlögl, U. Gas Sensing Performance of Pristine and Monovacant C_6BN Monolayers Evaluated by Density Functional Theory and the Nonequilibrium Green's Function Formalism. *J. Phys. Chem. C* **2020**, *124*, 5853−5860.

(33) Xiang, P.; Sharma, S.; Wang, Z. M.; Wu, J.; Schwingenschlögl, U. Flexible C6BN Monolayers As Promising Anode Materials for High-Performance K-Ion Batteries. *ACS Appl. Mater. Interfaces* **2020**, *12*, 30731−30739.

(34) Clementi, E.; Raimondi, D.-L. Atomic screening constants from SCF functions. *J. Phys. Chem.* **1963**, *38*, 2686−2689.

(35) Ayub, K. Transportation of hydrogen atom and molecule through $X_{12}Y_{12}$ nano-cages. *Int. J. Hydrogen Energy* **2017**, *42*, 11439−11451.

(36) Ayub, K. Binding affinity and permeation of $X_{12}Y_{12}$ nano-clusters for helium and neon. *J. Mol. Liq.* **2017**, *244*, 124−134.

(37) Pitt, I. G.; Gilbert, R. G.; Ryan, K. R. Application of transition-state theory to gas-surface reactions: barrierless adsorption on clean surfaces. *J. Phys. Chem.* **1994**, *98*, 13001−13010.

(38) Popa, I.; Fernández, J. M.; Garcia-Manyes, S. Direct quantification of the attempt frequency determining the mechanical unfolding of ubiquitin protein. *J. Biol. Chem.* **2011**, *286*, 31072−31079.

(39) Chen, R. J.; Franklin, N. R.; Kong, J.; Cao, J.; Tombler, T. W.; Zhang, Y.; Dai, H. Molecular photodesorption from single-walled carbon nanotubes. *Appl. Phys. Lett.* **2001**, *79*, 2258−2260.

(40) Zhang, Y.-H.; Han, L.-F.; Xiao, Y.-H.; Jia, D.-Z.; Guo, Z.-H.; Li, F. Understanding dopant and defect effect on H2S sensing performances of graphene: a first-principles study. *Comput. Mater. Sci.* **2013**, *69*, 222−228.

(41) Monshi, M. M.; Aghaei, S. M.; Calizo, I. Doping and defect-induced germanene: A superior media for sensing H_2S, SO_2, and CO_2 gas molecules. *Surf. Sci.* **2017**, *665*, 96−102.

(42) Mansouri, E.; Karamdel, J.; Berahman, M.; Ahmadi, M. T. Phosphorene as H_2S and CH_4 gas sensor. *Phys. Status Solidi.* **2019**, *216*, 1800086.

(43) Gui, Y.; Liu, D.; Li, X.; Tang, C.; Zhou, Q. DFT-based study on H_2S and SOF_2 adsorption on Si-MoS_2 monolayer. *Results Phys.* **2019**, *13*, 102225.

(44) Walia, G. K.; Randhawa, D. K. K. Adsorption and dissociation of sulfur-based toxic gas molecules on silicene nanoribbons: a quest for high-performance gas sensors and catalysts. *J. Mol. Model.* **2018**, *24*, 94.

(45) Huang, C.-S.; Murat, A.; Babar, V.; Montes, E.; Schwingenschlögl, U. Adsorption of the Gas Molecules NH_3, NO, NO_2, and CO on Borophene. *J. Phys. Chem. C* **2018**, *122*, 14665−14670.

(46) Aghaei, S. M.; Monshi, M. M.; Torres, I.; Zeidi, S. M. J.; Calizo, I. DFT study of adsorption behavior of NO, CO, NO_2, and NH_3 molecules on graphene-like BC_3: a search for highly sensitive molecular sensor. *Appl. Surf. Sci.* **2018**, *427*, 326−333.

(47) Aghaei, S. M.; Aasi, A.; Farhangdoust, S.; Panchapakesan, B. Graphene-like BC_6N nanosheets are potential candidates for detection of volatile organic compounds (VOCs) in human breath: A DFT study. *Appl. Surf. Sci.* **2021**, *536*, 147756.

(48) McCurdy, M. R.; Sharafkhaneh, A.; Abdel-Monem, H.; Rojo, J.; Tittel, F. K. Exhaled nitric oxide parameters and functional capacity in chronic obstructive pulmonary disease. *J. Breath Res.* **2011**, *5*, No. 016003.

(49) Simulator, Q. *Atomistix ToolKit (ATK)*; 2019.

(50) Grimme, S. Semiempirical GGA-type density functional constructed with a long-range dispersion correction. *J. Comput. Chem.* **2006**, *27*, 1787−1799.

(51) Landauer, R. Spatial variation of currents and fields due to localized scatterers in metallic conduction. *IBM. J. Res. Dev.* **1957**, *1*, 223−231.

(52) Buttiker, M. Coherent and sequential tunneling in series barriers. *IBM. J. Res. Dev.* **1988**, *32*, 63−75.